

LOCAL DEPOSITION SITES OF DRUG PARTICLES IN A HUMAN NASAL CAVITY

Kiao INTHAVONG, Zhao Feng TIAN, Hua Feng LI, Ji Yuan TU¹,
William YANG²,
Charlie XUE and Chuguang LI³

¹ RMIT, School of Aerospace, Mechanical and Manufacturing Engineering, Victoria 3083, AUSTRALIA

² CSIRO Minerals, Clayton, Victoria 3169, AUSTRALIA

³ RMIT, School of Medical Sciences, Victoria 3083, AUSTRALIA

ABSTRACT

Particle depositional studies from nasal sprays are important for efficient drug delivery. The main influences on deposition involve the nasal cavity geometry and the nasal spray device of which its parameters are controlled by the product design. It is known that larger particle sizes ($>>10\mu\text{m}$) at a flow rate of 333 ml/s impact in the anterior portion of the nose, leaving a significant portion of the nasal cavity unexposed to the drugs. Studies have found correlations for the spray cone angles and particle sizes with deposition efficiencies. This study extends these ideas to incorporate other parameters such as the insertion angle of the nasal spray and the injected particle velocity to observe its effect on deposition. A numerical method utilizing a particle tracking procedure found that the most important parameter was the particle's Stokes number which affected all other parameters on the deposition efficiency.

NOMENCLATURE

A_i	convective flux
a_1, a_2, a_3	constants for drag coefficient equation
C_D	coefficient of drag
D, d	diameter
\bar{d}	mean diameter
F_D	drag forces
g	gravitational acceleration
Re	Reynolds number
u	velocity
u^*	particle / gas velocity ratio
x_j	Cartesian coordinate system

Greek Letters

α	insertion angle
β	spray cone angle
Γ	diffusion coefficient
ν	kinematic viscosity
ρ	density
τ	particle relaxation time
ϕ	governing variable

Subscripts and Superscripts

g	gas phase
p	discrete particle phase
i	initial

INTRODUCTION

Nasal drug delivery is a popular way to treat respiratory ailments such as congestion and allergies. It has become an alternative to oral and injection routes of delivering systemic drugs for a variety of diseases and its advantages have been well documented. Information regarding particle deposition within the nasal cavity can be used for effective design of a nasal sprayer device to deliver drugs to specific targeted sites. Various studies adopting human subjects or nasal cavity replicas have found relationships for particle deposition efficiencies with nasal spray parameters, such as spray cone angle and the particle size distribution produced (Cheng et al. 2001, Suman et al. 1999). However, in-vivo and nasal cavity replica methods limit the scope of studies due to their tendency to be intrusive, time consuming and expensive to implement. Numerical analysis allows a wider range of studies (e.g. repeatability and accuracy of a nasal spray injection released from the same location) that is based on advancements in computational models employing Computational Fluid Dynamics (CFD) techniques (Hörschler et al. 2003).

Recent studies have measured spray characteristics, such as particle size and spray cone angle (Suman et al. 2002). A nasal spray produces drug particles in the range of $5\mu\text{m}$ up to $200\mu\text{m}$ with a mean of $45\text{-}65\mu\text{m}$ and spray cone angles ranging from narrow sprays at 35° degrees to wide sprays at 70° degrees. Newman et al. (1998) found that an increase in spray cone angle from 35° to 60° degrees showed a reduction in size of the deposition area as less of the spray was able to penetrate the narrow nasal valve. Cheng et al. (2001) found that deposition in the anterior region increased with an increase in cone angles. In contrast, Suman et al. (2002) found that there was not a significant difference in deposition patterns with respect to spray cone angles. It is argued that the changes in spray angle is unlikely to alter the distribution of droplets in the nose due to the narrow passageway of the nasal valve, compared with the spray plumes which are ten times greater. Thus the emitted plumes never have the opportunity to freely develop in the nasal cavity as they would in an unconfined space.

The differences in arguments stem from the numerous variations that exist in studying nasal spray deposition efficiencies (Tang et al. 2004). Moreover, the effects of the insertion angle of the spray device, the location of the insertion and the initial particle velocity were not discussed. It is the aim of this study to examine these

parameters and the influence it has on the deposition of particles in the nasal cavity by numerical analysis.

MODEL DESCRIPTION

Mesh Generation

A nasal geometry was obtained through a computed tomography (CT) scan of the nose of a healthy 25 year old, Asian male (170cm height, 75kg mass). The scans captured different positions from the entrance of the nasal cavity to just anterior of the larynx at intervals of 1 to 5 mm depending on the complexity of the anatomy. An initial model with 82,000 cells was initially used to solve the air flow field at a flowrate of 20L/min. The model was then improved by cell adaptation techniques that utilised local and solution based refinements, such as refining large volume cells, cells that displayed large velocity gradients and near wall refinements. This process was repeated twice, with each repeat producing a model with a higher cell resolution to the previous model. Subsequently four models were produced, 82000, 275000, 586000 and 822000. A velocity profile near the constricting nasal valve area was taken for each model and compared to check for grid independence. Figure 1 shows the velocity profile converge at a mesh resolution of 586,000 cells and a further increase to 822,000 cells showed no further improvement.

Numerical Models

A generic CFD commercial code, FLUENT 6.1.2, was used to predict the flow field of the continuum gas phase under steady-state incompressible conditions by solving the full Navier-Stokes equations. The flow was simplified as quasi-steady where the Strouhal number was much less than one based on an axial length taken from the entrance. The Reynolds number was calculated as 1378 which is low for turbulent internal pipe flows. However with the convoluted airway having bends and contraction-expansion regions, the presence of turbulent flow has been confirmed by Swift and Proctor (1977) and Schreck et al. (1993) where turbulent instabilities are found in the upper olfactory regions and in the expanding regions of the anterior turbinate region. Additionally Yan et al. (2004) assumed turbulent flow and used the k-ε turbulence model for flows around 200-300ml/s (Yan et al. 2004). The k-ε models are the most commonly used turbulence model known for their robustness and generality of use in engineering applications. It is based on the assumption of isotropic turbulence and a single eddy viscosity for all three components of the velocity vector that can cause inaccuracies for flows with high swirling action which makes the turbulence anisotropic. However for flows in the nasal cavity that exhibit low levels of swirl the k-ε approximation may be sufficient given the low computational costs compared with more sophisticated approaches such as Large Eddy Simulations and the Reynolds Stress Model. The gas phase Reynolds-Averaged conservation equations along with the equations for the turbulent kinetic energy and its dissipation rate can be cast in the general form:

$$\frac{\partial}{\partial x_j} (A_j \phi) - \frac{\partial}{\partial x_j} (\Gamma \frac{\partial \phi}{\partial x_j}) = S \quad (1)$$

with the coefficients representing the appropriate variable for the different governing equations.

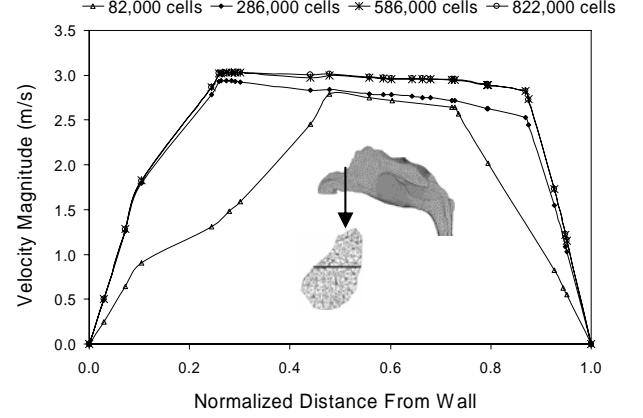


Figure 1: Velocity profiles at the nasal valve region for different nasal cavity models showing grid independence at 586000 cells.

Lagrangian Particle Tracking Model

A Lagrangian particle tracking method is used to trace the dispersion of particles about the trajectory. The Lagrangian scheme is combined with a stochastic Discrete Random Walk (DRW) scheme, albeit with high computational costs. Trajectories of individual particles can be tracked by integrating the force balance equations on the particle.

$$\frac{du_p}{dt} = F_D(u_g - u_p) + \frac{g(\rho_p - \rho_g)}{\rho_p} \quad (2)$$

$F_D(u_g - u_p)$ is the drag force per unit particle mass where

$$F_D = \frac{18\mu_g C_D \text{Re}_p}{\rho_p d_p^2 24} \quad (3)$$

where ρ_p denotes the density of particle material and d_p is the particle diameter. u_p presents the particle velocity.

Re_p is the particle Reynolds number defined as

$$\text{Re}_p = \frac{\rho_p d_p |u_p - u_g|}{\mu_g} \quad (4)$$

The drag coefficient C_D is given as:

$$C_D = a_1 + \frac{a_2}{\text{Re}_p} + \frac{a_3}{\text{Re}_p^2} \quad (5)$$

where the a 's are empirical constants for smooth spherical particles over several ranges of particle Reynolds number (Morsi and Alexander 1972).

However there are known problems with the DRW method in the way it takes into account the effects of turbulence. The method overestimates deposition for the smaller range of particles ($\ll 10\mu\text{m}$) due to the calculation of the normal Reynolds Stresses in the near wall region (Wang and James 1999, Zhang et al. 2004). This overestimation at the near wall region increases in sensitivity for smaller particles that have a shorter relaxation time. This effect is compounded by the geometry, which is similar to that of very narrow duct flows where the effects of the walls are emphasized. An improved model for the random walk method is proposed by Wang and James (1999). However, limitations in accessing and making the necessary modifications to the

commercial code FLUENT restricts the evaluation of this method. To overcome this, the present study incorporated a hybrid tracking method that uses both the DRW and mean flow tracking (which infers no turbulent particle dispersion) for the full particle size range.

Boundary Conditions

The nasal cavity was subjected to constant air flow rates of 10-40 L/min, where a laminar flow regime was implemented for the 10L/min case. The internal walls were modelled using an “enhanced wall treatment” function to consider the no-slip condition on the air flow. The particles adopted the properties of spherical water droplets, as most drug formulations are diluted with water. Initial particle conditions are assumed by analytical methods due to a lack of experimental data. The conditions for the release of particles into the constant flow rate differed for the parameter under investigation and are elucidated upon, within the relevant sections. The internal walls of the nasal cavity were set to a “trap” condition, meaning that particles touching a wall deposit at that location.

RESULTS

Validation using a Hybrid Method

A numerical hybrid tracking simulation was used where DRW tracking is used for larger particles where $I > 10,000$ and a mean flow tracking be used for $I < 10,000$, equivalent to $d_p \approx 5.5\mu\text{m}$ for a flowrate of 20L/min. The results were compared against Kelly et al. (2004) experimental results (Figure 2). The numerical hybrid tracking simulation overestimated deposition for $I < 10,000$ and underpredicted deposition for $I > 10,000$. One reason for the discrepancy is the intersubject variability between the nasal cavity models that Kelly et al. (2004) obtained (53 year-old non-smoking Caucasian male, 73kg mass, 173cm height) as opposed to the model used in the present study.

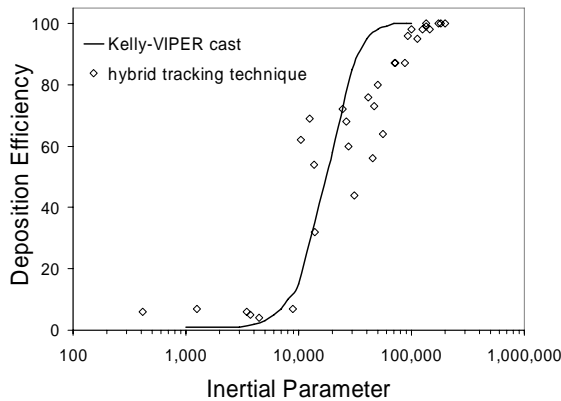


Figure 2: Deposition efficiency for monodisperse particles released passively from the nostril inlet subjected to airflow rates of 20L/min, 30L/min and 40L/min using a hybrid tracking technique.

Differences in the comparison of particle deposition efficiencies with the inertial parameter is discussed by Häußermann et al. (2002), such as the limitation of the inertial parameter not taking into account the changes in airway geometry. This constant air flow rate is a measure of the average impactability of the particle over the entire

domain, as it doesn't factor in the changes in velocity which is significant when the geometry under consideration is highly convoluted, narrow and complex. This provides some reasoning for variations in data for deposition efficiency versus inertial parameter charts.

Initial particle velocity

Monodispersed particles were released uniformly in a normal direction to the inlet surface of each nostril and the total deposition efficiency of particles impacting into Zone 1 and Zone 2 were recorded at different injected velocities.

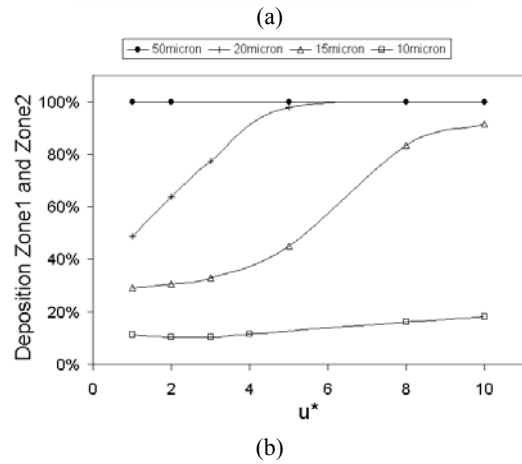
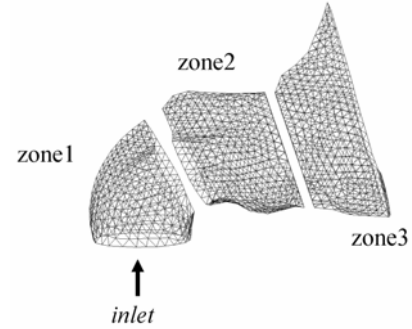


Figure 3: a) Segmented view of the front region of the nasal cavity showing Zone 1, 2 and 3. b) Total deposition efficiency in Zone 1 and Zone 2 of the nasal cavity for different particle injection velocity u^* , where $u^* = u_{pi} / u_g$

The injected particles have an increase in their kinetic energy, resulting in a higher initial momentum for the intended trajectory. However this energy is degenerated by the drag force acted on by the gas phase. The amount of influence the gas has on the particle is dependent on the particle Stokes number. Crowe et al. (1998) presents a relationship for the particle-gas velocity ratio as a function of the Stokes number:

$$u^* = \frac{u_p}{u_g} \approx \frac{1}{1 + St} \quad (6)$$

where

$$St = \frac{\rho_p d_p^2 U}{18\mu_g D} = \tau \frac{U}{D} \quad (7)$$

which suggests that for small Stokes numbers (i.e. $St \rightarrow 0$), the particle velocity approaches the gas phase velocity quickly. Large Stokes numbers (i.e. $St \rightarrow \infty$) suggests that u^* approaches zero. This means that the particle velocity is unaffected by the gas. It is expected that the dynamic

change in the particle velocity will occur within the frontal region of the nasal cavity given the order of magnitudes of the particles. This region is divided into three zones which conform to that of a 90° bend. The deposition of particles in Zone 1 and Zone 2 is investigated as the distance within these two zones is sufficient to capture the dynamic effects of sprayed particle conditions. Figure 3a shows the segmented Zones that exist in the frontal regions of the nasal cavity. Figure 3b shows the total particle deposition in the first two zones of the nasal cavity at different particle injection velocities.

Only a small influence on the impactability of a 10µm particle is observed when there is an increase in the initial particle velocity and this is seen by the slight increase in deposition. The lower Stokes number brings about a rapid decrease in velocity and the particle assumes the gas phase velocity before the change in direction of the flow. The influence of u^* amplifies as the particle size increases, where a large proportion of particles deposit more readily in the two frontal zones.

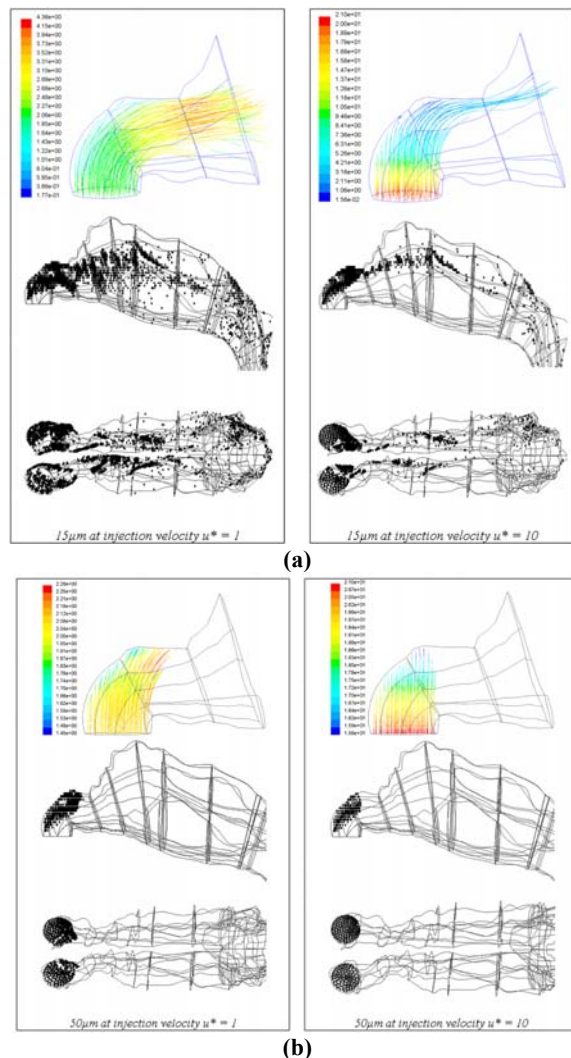


Figure 4: Particle trajectories coloured by velocity magnitudes (m/s) and local deposition sites for mono-sized particles released uniformly from the inlet surface normal to the nostril openings at $u^*=1$ and $u^*=10$. (a) 15µm particles and (b) 50µm particles.

About 70% of 15µm particles are able to follow the curved streamlines when $u^*=1$ as particle impactability is dominated by the Stokes number. However significant deposition increases when $u^* > 4$. The Stokes number, a ratio of the particle's relaxation time to the flow characteristic time, indicates how long it takes for the particle to adjust to the gas phase conditions. For a fixed distance (nostril opening to the top of the vestibule), an increase in u^* will decrease the time taken to cover this distance. This leads to a shorter time and distance for the particle to adapt to the gas phase conditions and presents a higher impactability than that calculated by the Stokes number alone. The influence of the injected particle velocity is still felt as the gas phase begins to curve. As particle size increases, so does the relaxation time that the particle needs to adapt to flow changes. As a result significant deposition increases occur at lower u^* values for larger Stokes numbers. The larger particles exhibit much higher Stokes numbers which prevents the particles from following the curved streamlines. It is observed that 50µm particles entrained in the flow ($u^*=1$) is an example of this. Therefore an injected 50µm particle ($u^*=10$) exhibiting a greater amount of initial momentum will only exacerbate the linear projectile motion of the particle. Thus it is evident that there are two forces acting against each other during the initial injection of the particles. The initial momentum force that is counteracted by the drag force which is inversely proportional to the particle Stokes number.

The particle trajectories for a low Stokes numbered-particle and a high-Stokes numbered-particle in comparison is shown in Figure 4a and b, respectively.

Insertion Angle (α)

The insertion angle, α , is the angle the nasal spray device makes away from the horizontal position, (0° in the x-y plane), when looking into the side of a person's face. Particle sizes of 10µm to 50µm were used at an initial velocity of 10m/s. A uniform surface injection released from the inlet was used to eliminate variables such as location of the nozzle tip, nozzle diameter and spray cone angle.

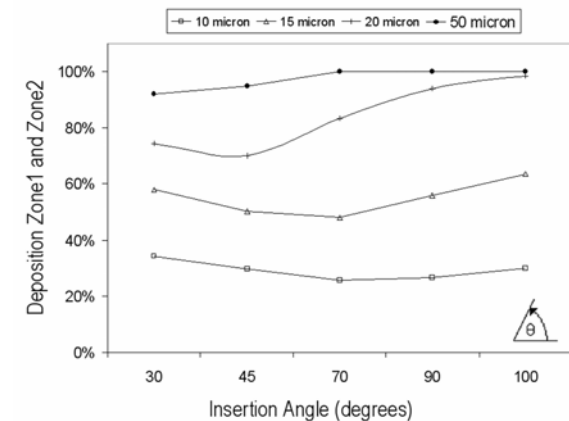


Figure 5: Deposition in zone1 and zone2 for monodispersed particles released uniformly from the inlet surface at 10m/s for different insertion angles.

Higher deposition occurred at 100° for most particles (Figure 5) as the particles are discharged directly into the anterior-most wall of the nasal cavity with an initial velocity of 10m/s. Minimum deposition for smaller sized

particles (10 μm and 15 μm) was found when $\alpha=70^\circ$. This direction of particles enhances the ability of turning, as more particles assume the streamlines that exist on the inside curvature. Less particles deposit vertically above the release point when $\alpha=70^\circ$ compared with $\alpha=90^\circ$. Further decreases in α , where the direction of discharge approaches the horizontal increases deposition of particles as a higher proportion of particles are now directed at the adjoining wall of the nostril, albeit a small margin. The deposition sites for $\alpha=30^\circ$ and $\alpha=70^\circ$ are similar in that particles that flow with the gas phase beyond Zone 3 will behave similarly, since at this stage the particle's initial momentum generated by the injection will have been dissipated by the drag force. However the concentration of particles depositing on the adjoining wall to the nostril inlet is much greater for $\alpha=30^\circ$ than $\alpha=70^\circ$ as shown in Figure 6.

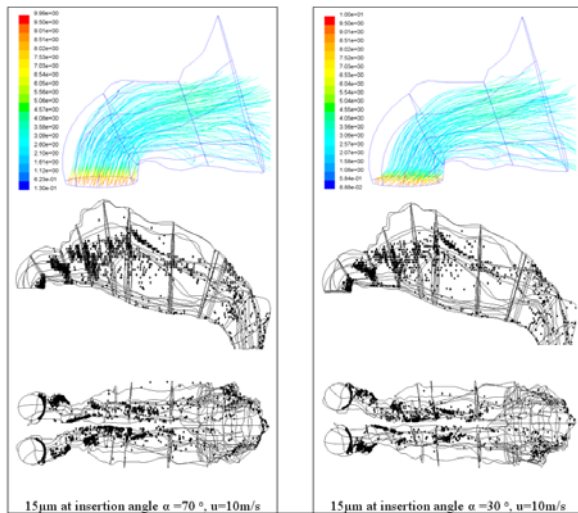


Figure 6: Particle trajectories coloured by velocity magnitudes (m/s) and local deposition sites for 15 μm particles released uniformly from the inlet surface at insertion angles 70° and 30°.

The deposition curves for 20 μm , behaves similarly to 10 μm and 15 μm particles, but at lower α (Figure 5). Minimum deposition in the two frontal zones was found at $\alpha=45^\circ$. Although more particles are directed into the adjoining wall, this is offset by more particles penetrating into the curvature instead of impacting straight into the roof of the vestibule as is the case when $\alpha=90^\circ$. These larger particles require a sharper angle of insertion to avoid impacting with the roof of the vestibule, thus aiding the alignment of the particles with the 90° bend and reducing the amount of deviation required in turning. The larger the particle (20 μm and 50 μm), the more effective the decrease in α is. Another insertion angle that can be considered is the orientation when looking into a person's face, front-on, in the y-z plane. This was not investigated as the same ideas regarding the particle size with its dependency on initial flow conditions exist.

Full Spray Cone Angle (β)

The full spray cone angle, β , is the dispersion of particles exiting from the nozzle tip. Particles had to be released from a small diameter compared with previous particle release, which used a uniform inlet release at the nostril openings, to allow observation of the physical differences when changing β . The initial particle velocity was 10m/s

from the centralised location of the nostril inlet, with a diameter of 0.8mm and a range of β between 20° to 80°.

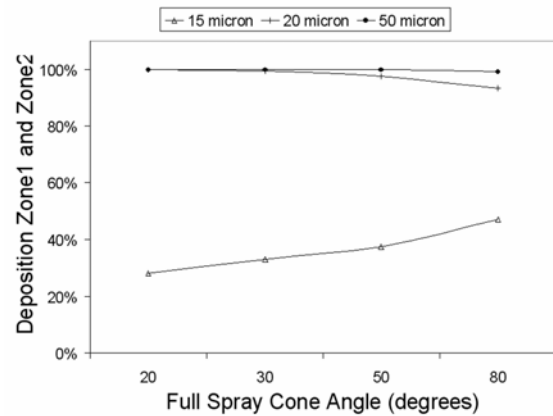


Figure 7: Total deposition in zone1 and zone2 for monodispersed particles released at 10m/s from a small internal diameter at the centre of the nostril inlet surface. The spray cone angles ranged from 20° and 80°.

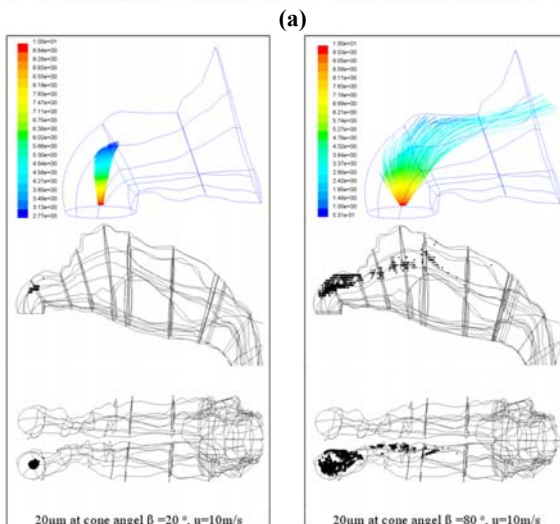
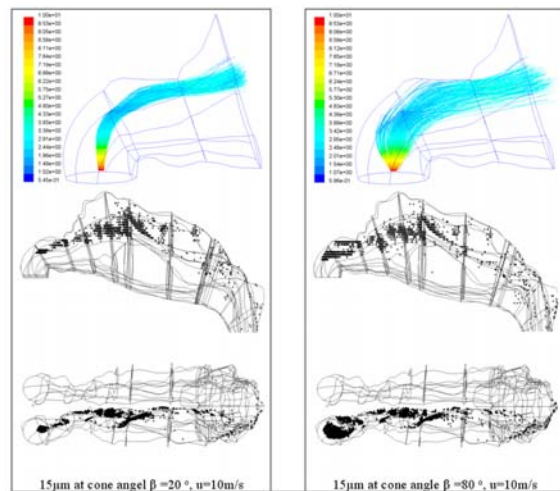


Figure 8: Particle trajectories coloured by velocity magnitudes (m/s) and local deposition sites for mono-sized particles released at 10m/s from a small internal diameter at the centre of the nostril inlet surface. The spray cone angles ranged from 20° and 80°. (a) 15 μm particles and (b) 20 μm particles released

The smaller ranged particles that follow the gas phase velocity more readily are optimised when released with a narrow β , as a wider β gives rise to a larger range of dispersion of particles due to the nature of a 360° spray cone. The larger dispersion creates a low ratio of favourably dispersed particles (those pointing with the flow) to those being dispersed away from the curvature (i.e. in the opposite direction) of the gas flow. The effect of this becomes apparent as particle size increases. Figure 8a shows the flow for $15\mu\text{m}$ being centralized when $\beta=20^\circ$ and the increase in deviation from the centre when $\beta=80^\circ$. Deposition for $\beta=20^\circ$ remains along the roof of the nasal cavity and near the septum walls with 28% depositing in the first two zones. At $\beta=80^\circ$ deposition in the two frontal zones is increased to 47%, where a larger deposition area, due to the particle dispersion, occurs.

The internal location of injection is closer to the roof of the vestibule than from the surface nostril inlets. This reduces the allowable distance for particles to relax their initial conditions to the gas phase conditions, thus enhancing impaction on the roof of the vestibule. As seen earlier $20\text{--}50\mu\text{m}$ particles have near 100% deposition in the front two zones. Subsequently any particle dispersion that is favourable will project the particles into the already curved streamlines, allowing them to travel further, albeit a small distance. Figure 8b compares the two deposition patterns for $20\mu\text{m}$ particles at $\beta=20^\circ$ and $\beta=80^\circ$. At $\beta=20^\circ$, impaction occurs directly above the injection release point in a concentrated area. When $\beta=80^\circ$, a wider area of deposition is observed in the frontal zones, whilst those particles projected favourably towards the nasal valve are able to travel beyond the 90° bend. However its deposition is imminent and this occurs within the middle sections of the nasal cavities. Therefore an optimum β , is based on the ratio of the change in favourably dispersed particles to the number of particles that are predestined to impact on the roof of the vestibule because of their particle size.

CONCLUSION

This study demonstrates the significant influence the Stokes number plays in deposition of particles in the nasal cavity. For a flow rate of 20 L/min $10\text{--}20\mu\text{m}$ particles were sensitive to initial injection velocity, insertion angle, and spray cone angle. Larger particles exhibited very high Stokes numbers which caused them to be insensitive to these parameters.

Current commercially available nasal sprays produce mean size particles of $45\text{--}60\mu\text{m}$ which presents a problem as larger particles ($\geq 20\mu\text{m}$), are relatively insensitive towards initial injection conditions and are likely to deposit in the anterior portion of the nose decreasing the drug delivery's efficiency. Producing smaller particles ($\leq 20\mu\text{m}$) during atomisation is an option for designers, however smaller particles are more inclined to follow the gas phase flow, which can lead to deposition beyond the nasal pharynx.

The ideas formulated can be used as a basis for improving the design of nasal spray devices to achieve better drug delivery such as (i) redirecting the release point of the spray (i.e. the insertion angle) to be align with the flow streamlines (ii) controlling the particle size distribution and (iii) controlling the particle's initial velocity. In the attempt to replicate actual nasal spray applications whilst isolating

the investigating parameters, idealized injected conditions for the particles were used, along with the idealized nasal cavity. Further studies are needed to extend the results to other nasal cavities, to include the permeability effects of nasal hairs, and establishing more accurate initial particle conditions such as the instantaneous velocity at injection that can include swirl effects.

ACKNOWLEDGEMENTS

The financial support provided by the Australian Research Council (project ID LP0347399) is gratefully acknowledged.

REFERENCES

- CHENG, Y.S., HOLMES, T.D., GAO, J., GUILMETTE, R.A., LI, S., SURAKITBANHARN, Y., ROWLINGS, C. (2001). Characterization of Nasal Spray Pumps and Deposition Pattern in a Replica of the Human Nasal Airway, *J. Aerosol Med.* 14(2): 267-280.
- CROWE C., SOMMERFELD M., TSUJI Y., (1998). Multiphase Flows with Droplets and Particles, *CRC Press LLC*, USA: p.25
- HÄUBERMAN, S., BAILEY, A.G., BAILEY, M.R., ETHERINGTON, G., YOUNGMAN, M. (2001). The influence of breathing patterns on particle deposition in a nasal replicate cast. *J. Aerosol Sci.* 33: 923-933.
- HÖRSCHLER, I., MEINKE, M., SCHRÖDER, W. (2003). Numerical Simulation of the Flow Field in a Model of the Nasal Cavity, *Comput. Fluids.* 32: 39-45.
- KELLY, J.T., ASGHARIAN B., KIMBELL, J.S., AND WONG, B.A. (2004). Particle Deposition in Human Nasal Airway Replicas Manufactured by Different Methods. Part 1: Inertial Regime Particles, *Aerosol Sci. Technol.* 38: 1063-1071.
- NEWMAN, S.P., MOREN, F., CLARKE, S.W. (1998). Deposition Pattern of Nasal Sprays in Man, *Rhinology.* 26: 111-120.
- SUMAN, J.D., LAUBE, B.L., LIN, T.C., BROUET, G., AND DALBY, R. (2002). Validity of in Vitro Tests on Aqueous Spray Pumps as Surrogates for Nasal Deposition, *Pharma. Res.* 19: 1-6.
- SCHRECK S., SULLIVAN K. J., HO M., CHANG H.K., (1993) Correlations between flow resistance and geometry in a model of the human nose, *J Appl Physiol.* 75 (4): 1767-1775
- SWIFT, D.L., and PROCTOR, D.F. (1977) Access of air to the respiratory tract, *Respiratory Defense Mechanisms*, Brain J.D., Proctor D.F., and Reid L.M., eds., Marcel Dekker Inc., New York, pp 63-91
- TANG, H., TU, J.Y., ABU-HIJLEH, B., XUE, C., LI, C.G. (2004) Dynamic analysis of airflow features in a 3d real-anatomical geometry of the human nasal cavity. *Proceedings of the 15th Australasian Fluid Mechanics Conference*, Sydney, Australia
- WANG, Y AND JAMES, P.W. (1999) On the effect of anisotropy on the turbulent dispersion and deposition of small particles, *Int. J. of Multiphase Flows* 25: 551-558.
- YAN, J., KARANJKAR, J.A., BRANAGAN, M. 2004. Dynamic modelling and simulation for nasal drug delivery. *PMPS-Drug Delivery*: August-2004: 68-71.
- ZHANG, Y., FINLAY, W.H, MATIDA, E.A. (2004) Particle deposition measurements and numerical simulation in a highly idealized mouth-throat, *J. Aerosol Sci.* 35: 789-803.